Single bubble dynamics during nucleate flow boiling on a vertical heater: Experimental and theoretical analysis of the effect of surface wettability,roughness and bulk liquid velocity

Sarker, D.; Ding, W.; Schneider, C.; Hampel, U.;

Publiziert:

Juli 2019

International Journal of Heat and Mass Transfer 142(2019), 118481

DOI: https://doi.org/10.1016/j.ijheatmasstransfer.2019.118481

Perma-Link zur HZDR-Publikationsdatenbank

https://www.hzdr.de/publications/Publ-29570

Single bubble dynamics during nucleate flow boiling on a vertical heater: Experimental and theoretical analysis of the effect of surface wettability, roughness and bulk liquid velocity

D. Sarker[a], W. Ding[a,b], C. Schneider[c], U. Hampel[a,b]

[a] Helmholtz-Zentrum Dresden-Rossendorf (HZDR), Institute of Fluid Dynamics, Bautzner Landstraße 400, 01328 Dresden, Germany

[b] Technische Universität Dresden, Chair of Imaging Techniques in Energy and Process Engineering, 01062 Dresden, Germany

[c] University of Applied Sciences Zittau/Görlitz, Institute of Process Technology, Process Automation and Measuring Technology, 02763 Zittau, Germany

Abstract

The present study reports the mutual effect of heater surface wettability, roughness and bulk liquid velocity on the bubble dynamics and departure in nucleate boiling. Boiling experiments were conducted at atmospheric pressure with degassed-deionized water at low subcooling (1.9 ± 0.25 K) for vertically oriented stainless steel heaters. Self-assembled monolayer (SAM) coating and wet-etching technique were used to alter the heater surface wettability and roughness. Liquid contact angle hysteresis (θ_{hys}) and root mean square roughness (Sq) of the heater surfaces were adjusted between $42.32° \leq \theta_{hys} \leq 68.56°$ and roughness $0.01\ \mu m \leq Sq \leq 0.549\ \mu m$. High resolution optical shadowgraphy has been used to record the bubble life cycle. Experimental results show that higher bulk liquid velocity yields smaller bubble departure diameters for all heater surface characteristics. Bubble departure diameters are greater for low wetting surfaces. The bubble growth rate and departure diameter were found maximum for an intermediate surface roughness Sq between 0.108 and 0.218 μm. The corresponding roughness height is referred to as the 'optimal roughness height' in this study. Eventually, a bubble departure criterion was derived from the expressions of forces which act on a nucleating bubble throughout its growth cycle. 90% of the departing bubbles satisfy the bubble departure criterion with ± 25% deviation.

Keywords: bubble growth, bubble departure, surface wettability, roughness, flow boiling.

Nomenclature

C_{eff}	constant, quantifying the effect of heater surface characteristics on bubble growth	ΔT_{sub}	subcooling temperature (K)
		ΔT_w	wall superheat (K)
c_p	specific heat capacity (J/kgK)	θ	liquid contact angle (°)
d_w	bubble base diameter (m)	ϕ	bubble inclination angle (°)
D	diameter (m)	ν	kinematic viscosity (m^2/s)
f	bubble frequency (1/s)	ρ	density (kg/m^3)
F	force (N)		
g	gravitational acceleration (= 9.81 m/s^2)	*Subscripts*	
G_s	non-dimensional liquid shear gradient		
h	heat transfer coefficient (W/m^2K)	*adv*	advancing
h_{lv}	latent heat of evaporation (J/kg)	*b*	bubble
k, K	thermal conductivity (W/mK), area influential factor	*c*	condensation, conduction
		cm	center of mass
m	constant, fraction of the bubble height	*d*	departure
N_n	nucleation site density ($1/m^2$)	*eff*	effective
Nu	Nusselt number	*eq*	equivalent
Pr	Prandtl number	*ev*	evaporation
q''	heat flux density (W/m^2)	*fc*	forced convection
r	radius (m)	*g*	growth
Re	Reynolds number	*hys*	hysteresis
Sq	root mean square roughness of surface (μm)	*i*	interface
St	maximum roughness height of surface (μm)	*l*	liquid
t	time (s)	*ml*	microlayer
T	temperature (K)	*qc*	quenching
		rec	receding
Greek symbols		*v*	vapor
		w	heater wall, waiting period
α	advancing bubble contact angle (°)	*x*	normal to the heater wall
β	receding bubble contact angle (°)	*y*	upward direction
δ	thermal liquid layer thickness (m)		

1. Introduction

1.1 Motivation

Nucleate boiling is one of the most important modes of heat transfer. It which involves complex mass, momentum and energy transfers which take place at the interfaces (solid-gas, solid-liquid,

liquid-gas, gas-liquid-solid) and the bulk [1]. Different parameters, such as fluid properties, subcooling, bulk liquid velocity, system pressure etc. have effect on the bubble dynamics. Mass flux and system pressure are found as very influential to the bubble departure [2] and nano-micro patterned surfaces [3, 4] have significant role on the boiling heat transfer. Hence investigating the impact of heater surface characteristics and bulk liquid velocity on a single nucleated bubble is crucial for further scientific understanding and optimization of boiling heat transfer. The study reported in this paper was performed to investigate the mutual influence of heater surface wettability, roughness and bulk liquid velocity on the bubble dynamics and departure in nucleate boiling. The total evaporative, quenching and convective heat flux in nucleate boiling are:

$$q''_{ev} = \frac{\pi}{6} D_d^3 \rho_v h_{lv} f N_n . \quad [5] \quad (1\text{ a})$$

$$q''_{qc} = 2\sqrt{\frac{k_l \rho_l c_{p,l}}{\pi t}} \left(T_w - T_{sat}\right) t_w f K \frac{\pi D_d^2}{4} N_n . \quad [6] \quad (1\text{ b})$$

$$q''_{fc} = h_{fc} \left(\Delta T_w + \Delta T_{sub}\right) K \left(1 - \frac{\pi D_d^2}{4}\right) N_n . \quad [7] \quad (1\text{ c})$$

Here, K is a bubble influence factor which was suggested as $K = 0.5$ in a recent study [8]. Among the different parameters of the bubble ebullition cycle the bubble departure diameter (D_d) is one of the most important ones (Eqns. 1 a, b, c) as it is associated with latent heat. Eqn. 1 (a) shows that the total latent evaporative heat transfer (q''_{ev}) has a cubic dependency on the bubble departure diameter and thus a slight uncertainty of this parameter can notably deteriorate the accuracy of the total heat transfer calculation. The departing bubble also has a strong influence on the transient conduction heat transfer. Quenching heat transfer (q''_{qc}) due to the transient heat conduction was found to dominate the total heat transfer [7]. Usually, the contribution of the liquid phase convective heat transfer (q''_{fc}) to the total heat transfer is less [7]. Thus, it can be concluded that the departure dynamics of an isolated nucleated bubble is crucial for the estimation of the wall boiling heat transfer. Therefore, in the following, the basic physics of the bubble departure process will be explained.

1.2 Physical process of bubble departure

In simple words, the bubble departure criterion can be defined as a condition in which a growing bubble leaves the cavity and the cavity mouth is free for the growing of a subsequent bubble. Hence it can be defined by the condition $y_{cm} > r_w$ where the bubble inclination angle is assumed to be

related with the movement of apparent contact lines of the bubble base. High resolution optical observations manifest that the bubble departure comprises of complex mechanisms. Jung and Kim [9] observed the complete depletion of the microlayer beneath the nucleated steam bubble on a horizontal surface during the growth period and then, that the bubble base shrank. The shrinkage of the bubble base was followed by departure [10]. Pool boiling on a vertical surface is more complicated than on a horizontal surface, because the bubbles grow at an angle with respect to the heater surface in response to the upward buoyancy force. Therefore, forces acting on the bubbles are directed normal and parallel to the heater wall. In this case, bubbles may depart from the nucleation site by sliding, which is not the case for pool boiling on a horizontal heater [11]. The departure of a steam bubble is appreciably more complex in flow boiling conditions.

The bubble departure criterion is often derived using force balances [2, 12]. Table 2 summarizes the equations of different forces and Fig. 2 shows their directions. The forces, such as buoyancy (F_b), unsteady drag (F_{du}), quasi-steady drag (F_{qs}), surface tension (F_s), additional-added mass ($F_{growth,\ bulk}$), shear lift (F_{sl}), contact pressure (F_{cp}) and hydrodynamic pressure (F_h) force were well explained by several investigators [2, 11-14]. When the sum of the forces along the flow direction is just greater than zero, then the bubble departs. Klausner et al. [13] compared F_{sx} and F_{qs} for flow boiling conditions and argued that F_{sx} is not sufficient to prevent a vapour bubble from departure. Due to the asymmetrical bubble growth on the heater surface, liquid drag on the bubble surface exhibits an unsteady drag force (F_{du}). This force may act opposite to the flow direction and is important in holding the bubble at its nucleation site prior to departure. Thorncroft et al. [11] introduced an additional-added mass force ($F_{growth,bulk}$) which is associated with the bubble growth for flow boiling, acts entirely in the positive *y*-direction and assists the bubble departure. The bubble-liquid interface experiences a quasi-steady drag force (F_{qs}) due to the bubble velocity (V_b) relative to the bulk liquid velocity (V_l) that acts parallel to the flow direction. F_{qs} was suggested as the dominant force for the bubble departure condition on a horizontal heater surface by Klausner et al. [13]. Chang [15] combined the static forces (F_b, F_s) with the dynamic forces (F_{qs}, F_{sl}) to develop a bubble departure criterion for flow boiling on an inclined surface. The significant forces for the bubble departure on vertical heaters in Cho et al. [16] were supposed to be F_b, F_s, F_{du} and F_{qs}. Sugrue and Buongiorno [5] performed a sensitivity analysis to find out the dominant forces for different mass fluxes. The bubble departure mechanism was found to be sliding for low mass flux where F_b and F_{sy} are dominant. For a high mass flux regime, F_{sx} and F_{sl} were found more influential for the bubble detachment.

1.3 Effect of heater surface characteristics and bulk liquid velocity on bubble departure

The impact of heater surface characteristics on the bubble dynamics may be understood through the thermo-hydrodynamics of the microlayer beneath a nucleated bubble. Numerous groups employed the shadowgraph imaging technique to investigate the effect of heater surface wettability [17-21] and roughness [22-24] on the bubble dynamics and departure for pool and flow boiling. Phan et al. [17] found larger bubbles and lower bubble emission frequencies for the well-wetting surfaces. Bubble departure diameters were found almost 3 times larger on the hydrophobic surface [18] and 2 times smaller on the hydrophilic surface [19] compared to the uncoated silicon surface for horizontal pool boiling. Rousselet [20] studied the effect of heater surface wettability on the bubble departure diameter for a wide range of bulk liquid velocities (0 - 0.30 m/s) but his findings were inconclusive. Bubble sliding velocities were found greater [22] and the sliding distances were shorter for well-wetting surfaces [20, 22]. Bubble base diameters were found to increase for the surfaces with larger liquid contact angle [22]. Jo et al. [25] claimed that the direction of the surface tension at the triple-point (three-phase intersection) is towards the generated bubble side for the hydrophilic cases and outward of the vapor bubbles for the hydrophobic cases. Therefore, a hydrophobic heater surface results in a larger contact area than a hydrophilic surface. Consequently, larger bubbles are generated on the hydrophobic surfaces. Roughness, though being one of the main parameters of surface characteristics, has been so far a lesser subject of investigations according to the available literature. However, it can be hypothesized that even small-scale increase of surface roughness may increase the evaporative heat transfer area, as the ratio of actual to projected surface area is higher for rough surfaces. Kruse et al. [26] fabricated surface structures via a femtosecond laser surface processing technique. The influence of surface roughness (Rq = 1.4-7.8 μm) on the heat transfer coefficients at lower heat flux were not conclusive in their study. Goel et al. [23] studied the effects of stainless steel surface roughness (Ra = 0.50-3.54 μm) on the bubble departure for subcooled nucleate pool boiling. They found that the departure diameter decreases as the surface roughness increases. They did not addressed the interactions of the heater surface profile and the microlayer dynamics, though they are important [27]. Kim et al. [4] observed a larger bubble size and a lower bubble frequency on the designed surface structure due to the trapped superheated liquid layer between the microstructures. Zou et al. [3] reported an early evaporation of microlayer beneath the bubble base. An almost 5.25 times higher bubble growth rate was found on the ridge-structured surface compared to a plain surface. Sarker et al. [22, 27] found that the heat transfer to the bubble was the greatest due to the maximum microlayer evaporation rate at an intermediate roughness height.

The bulk liquid velocity is another important parameter that impacts the bubble dynamics. Several studies asserted that for higher bulk liquid velocity the bubble growth rate and the departure diameter decrease [2, 20, 28]. The bubble growth rate significantly influences the departure diameter and they are positively correlated [20]. One of the reasons for decreasing the bubble growth rate could be that the increase of bulk liquid velocity leads to a decrease in thermal boundary layer thickness on the heater surface which decreases the heat diffusion to the bubble [20]. Yoo et al. [29] performed experiments for HFE-301 on vertical ITO film heaters for upward subcooled flow boiling conditions. Their findings are in agreement with other groups [2, 30]. That is, bubble size and axial bubble velocity decreased and the bubble release frequency increased with the increase of bulk liquid velocity. Condensation heat transfer on the bubble surface due to the bulk liquid velocity also affects the bubble departure diameter. Condensation rate increases with the bulk liquid velocities, thus bubble growth rate and bubble departure diameter may decrease.

The literature survey concludes that heater surface wettability, roughness and bulk liquid velocity have significant impact on the bubble departure. However, mutual influence of these parameters on the bubble dynamics was not investigated in the above-mentioned studies. Moreover, existing bubble departure models do not account the role of heater surface characteristics. Currently the force balance approach is extensively used to define a bubble departure criterion, though the expressions for different forces consist of empirical constants. Therefore, experiments have been performed in this work to take into account the simultaneous impact of these parameters (surface wettability, roughness and bulk liquid velocity) on the bubble departure for vertically oriented heaters. The article is structured as follows. Section 2 delineates the surface preparation techniques for the examined heater surfaces, the experimental setup, measurement techniques, experimental procedure and relevant uncertainties. Section 3 discusses the experimental findings for the role of surface characteristics and bulk liquid velocity on the bubble dynamics and departure. We have formulated a simpler expression for the bubble departure criterion in section 4. Section 5 eventually summarizes the results and gives a general outlook.

2. Experiment

In order to stay close to the practice, 0.5 mm thick stainless steel heater plates were used in the experiments, as steel is common in many heat transfer applications. The thermal conductivity and the electrical resistivity of the used stainless steel material were 15 W/mK and 0.73 Ω mm²/m at 20°C, respectively. The deposition of chemicals on surfaces also modifies the surface wettability. Self-

assembled monolayer (SAM) coating, chemical vapor deposition (CVD) or oxidation technique can change the surface wettability without altering the roughness noticeably. Deposition of ultrathin layers is one of the reliable methods for influencing the surface wettability and investigating the isolated bubble dynamics in nucleate boiling. In total, 9 different test surfaces were treated by various techniques in order to get a range of surface wettability and roughness in the present study. The surface preparation methods, which were used are wet-etching and self-assembled monolayer (SAM) coating. A surface roughness height (*St*) of less than ~5 μm is suitable for investigating isolated bubbles in nucleate boiling. This limit of surface profile height was found during experiments in this work for a wide roughness range. A surface profile height with more than 5 μm may act like bubble nucleation cavities. Geometry and shape of a cavity were kept constant, to nullify their effect on the bubble dynamics. The surface preparation and analyzing techniques are explained below.

2.1 Surface preparation and analyzing

All the test surfaces were mirror polished with root mean square roughness $Sq \leq 0.01$ μm prior to employment of other surface treatment techniques. Wet-etching was used to control the roughness of surfaces. 6 stainless steel surfaces were etched by dipping polished samples in an acid solution (H_2O: HCL: HNO_3 = 6:6:1) for a time period in the range of 5 to 35 mins at room temperature. Generally, surfaces get rougher when dipping periods are longer. The acidic solution of wet-etching method removes a layer of material from the surfaces. Therefore, the roughness of a wet-etched surface does not solely depend on the etching period and the chemical composition of the solution, but also on the elemental composition, grain size and orientation of the solid material. The self-assembled monolayer (SAM) coating was used to modify the wettability of 4 stainless steel surfaces. Among 4 of these samples, 2 were mirror-polished and other 2 were wet-etched. SAM is done by depositing a layer of molecules on a substrate by simply dipping it in a special liquid solution. According to literature, the monolayer is ultra-thin and the length of a formed C-C single bond is about 0.15 nm. An SAM layer is about 10 carbon atoms, which is around 1-1.5 nm thick. As the thickness of SAM coating is in the nanometer scale, it does not influence the roughness of surfaces notably. The SAM coating method explained in Harm et al. [31] was applied in this study to modify the wettability of surfaces. Polished and rough surfaces were coated by Heptadecafluorodecylphosphonic acid (HDPA) (CAS 80220-63-9) and Etidronic acid (EDA) (CAS 7414-83-7) to decrease and increase the surface wettability, respectively.

The surface wettability was assessed using a goniometer (DataPhysics OCA 30) following the dynamic liquid contact angle measurement method rather than the static liquid contact angle. Dynamic liquid contact angles were measured following the sessile drop method. Thus, both the advancing θ_{adv} and receding θ_{rec} liquid contact angles of the treated surfaces were captured. The liquid contact angle hysteresis is calculated as $\theta_{adv} - \theta_{rec} = \theta_{hys}$. The liquid contact angle hysteresis is the results of the pinning effect of the three-phase contact line. The significance of liquid contact angle hysteresis to characterize a surface has been extensively investigated by different groups and they concluded that it arises from the surface roughness and/or heterogeneity [32]. A non-contact optical method namely confocal microscopy (μsurf expert, xy-resolution: 0.3-3μm, z-resolution: 3 nm) was used to analyze the surface topography. The images of surface topography were obtained with a 50x lens over an area of 320 μm x 320 μm. From these images, the 2D and 3D profiles were created and the roughness parameters (*Sa*, *Sq*, *St* etc.) were calculated in accordance with the international standard ISO 25178. The measurement errors arising from noise and slight vibrations of the surroundings were reduced during analysis by setting the z thresholds carefully. The details of surface preparation techniques and the corresponding surface wettability and topology information are shown in Fig. 2.

Two polished surfaces were coated with the HDPA and EDA and yielded θ_{hys} = 65.30° and θ_{hys} = 42.32°. The liquid contact angle hysteresis of the uncoated polished surface was 49.22°. Thus, we obtained 3 different wetting surfaces where roughness effect on the boiling is negligible. We found that the surface roughness increased with the etching duration (Fig. 2). The minimum etching period was 5 mins and the maximum one was 35 mins which produce a *Sq* of 0.108 μm and 0.549 μm. Monolayer coatings were also deposited on two rough surfaces (*Sq* = 0.266 μm and 0.392 μm) to change the wetting characteristics of them. The HDPA and EDA coatings on the surfaces with *Sq* = 0.266 μm and *Sq* = 0.392 μm gave a liquid contact angle hysteresis of θ_{hys} = 68.55° and θ_{hys} = 45.95°, respectively. Test surfaces had different roughness (*Sq* = 0.108, 0.218, 0.406 and 0.549 μm) which θ_{hys} is 59.97°±1.50°. However, this study addresses the role of heater surface roughness (*Sq* in the range from ~0.01 to 0.549 μm) and surface wetting characteristics on the bubble dynamics. The surface wettability and roughness has been measured at 6 different locations on the surfaces for each kind of preparation. The surface roughness and wettability were measured before and after the boiling experiments. The averaged values of these two measurements of the samples are used to characterize the surfaces. With the increase of surface roughness height deviations of surface profile measurement are increased. The deviations of *Sq* and *St* for polished surfaces were determined as

± 0.00195 µm and ± 0.036 µm and for rough surfaces, they were ± 0.0275 µm and ± 0.285 µm, respectively. The measurement of liquid contact angle also gives some uncertainty. The maximum deviations for advancing liquid contact angle and liquid contact angle hysteresis were found to be ± 2.952° and ± 4.109°. Test samples were cleaned before measuring the surface parameters (liquid contact angle and surface roughness) and using them in the boiling experiments. Surfaces were cleaned in an ultrasonic bath with ethanol at 40°C for 30 minutes. Liquid ethanol on the test surfaces was dried by a nitrogen flow just after taking out the samples from the ultrasonic bath. To initiate nucleate boiling in a well-defined position, a cylindrical artificial cavity of approximately 1963.5 µm² and 50 µm depth was prepared by the microlaser. The deviations in the preparation of the cavity diameter were determined as ± 8.00%. The total size of the heater which was used in the boiling experiments was 130 x 20 mm².

2.2 Flow boiling experiments and measurement techniques

A subcooled flow boiling loop was used for investigating the isolated bubble dynamics in upward flow boiling experiments. The experiment was conducted at 1 atmospheric pressure using deionized water. A schematic diagram of the flow boiling loop is shown in Fig. 3. The test facility was constructed earlier for a nucleate boiling experiment [33]. For the present study, the test section and the flow meter with its connections of the loop were modified. The main components of the flow loop were a pump, a preheater, a flow meter, a degasser, a filter, an air-cooled condenser and a test section (see Fig. 3). A special pump with low net positive suction head (NPSH) of lower than 0.5 m at 6 m³/h was used to circulate the test fluid. An electric preheater of 10 kW was installed downstream of the pump and before the flow meter with a bypass valve to control the liquid subcooling at the inlet of the test section. The electric power of the preheater was sufficient to maintain the inlet liquid temperature close to the saturation temperature. The mass flow rate was measured using a Krohne Optimass 1400 C Coriolis mass flow meter. The maximum range of the flow meter was 1.806 kg/s with an accuracy of better than ± 0.20% of the actual measured value.

Fig. 4 shows the details of the test section. The test section comprises a 28 mm x 28 mm x 350 mm rectangular flow channel. Three sides of the test section were made of borosilicate glass for optical access to the heating surface. The rear panel of the test section consists of a stainless steel frame, a block of thermal insulating polyether ether ketone (PEEK) which fixes the test heaters, the copper connections for heating the heaters by the electric power and the treated stainless steel heaters themselves. The thermal conductivity and the specific volume resistivity of the PEEK are 0.25

W/m.K and 10^{16} ohm-cm, respectively. Before fixing the PEEK block with the test heaters in the stainless steel frame, temperature resistant silicon paste (thermal conductivity 0.18 W/m.K) was used to glue the gaps between the test samples and the PEEK block. The back panel of the test section was fixed and sealed properly with the borosilicate glass parts. A narrow channel was fabricated in the PEEK block and a K-type thermocouple was inserted through the narrow channel which touched the back side of the test heater surfaces for measuring the heater wall temperature.

The loop was flashed and rinsed with deionized water and acetone before performing the experiments. At that time, the water which flows through the loop was filtered as well to remove impurities if there were any. The loop was then filled up with deionized water. The entrapped gases in the different components of the loop were released with the help of valves and the loop was completely filled up with water. Then the boiler was turned on for degassing the liquid. The deionized water in the boiler was heated up to saturation temperature for more than 2 hours without fluid flow. For further degassing, the water was pumped through the loop at low flow velocity and low subcooling. The pump and the preheater were keep running for some time, so that the dissolved gases would be removed completely. This process took around 1 hour. When the liquid was sufficiently degassed, the power source was switched on to generate bubbles from the artificial cavity. The test heaters were operated for some time to get rid of entrapped gases in the cavities of the surfaces. The heating power was in the range of 39.41 kW/m² - 45.47 kW/m². The desired bulk liquid velocities were obtained by adjusting the bypass valves and the rotational speed of the pump, which were measured by the flow meter. It is worth mentioning that special care was taken to keep the stainless steel heater surfaces clean. Once the bulk liquid velocity and the bubble ebullition cycle were in steady state, the data was collected. The temperatures of the liquid at the inlet and outlet of the test section were measured by the calibrated K-type thermocouples. The liquid subcooling at the inlet of the test section was set to 1.9 ± 0.25 K with the help of the preheater. For each test run, the bulk liquid velocity and the heating power were adjusted. Thus the heating power and the flow rate were acquired. Also, the inlet and outlet temperatures of the test section and the heater wall temperature were measured.

High resolution optical shadowgraphy using a MotionPro high-speed video camera (1280 x 1024 pixels and 1030 frames per second) equipped with an AF Micro-Nikkor 105 mm f/2:8D lens was employed for recording the bubble life cycle. A wide-open aperture (f/2.8) provides a shallower depth of field and the bubbles were focused and captured in this mode. This way, sharp bubble images were obtained while all background structures have been blurred out. The recording

speed of the camera was 2,500 frames per second while the spatial resolution was 16.40 ± 1.50 μm per pixel. The stacks of images from the high-speed video camera were processed using the image processing software ImageJ. The major steps of image processing are explained in other articles [22, 24]. The bubble base diameters were estimated in this study as well. For that, the temporal evolutions of the vapor bubble-solid interfaces were captured using a tool of the ImageJ called 'Orthogonal views'. A simple Matlab script was written to evaluate the bubble departure diameters in terms of the bubble base radius and the center of mass of a bubble in the upward direction.

2.3 Uncertainty analysis

Optical shadowgraphy has several sources of uncertainty. Apart from the static uncertainty of the camera sensor, the imaging technique has got a spatial uncertainty which was estimated from the pixel resolution. Another source of uncertainty is the geometry analysis of the bubbles. Altogether, the uncertainty of imaging is ± 0.0409 mm. The thermocouples were calibrated against a reference thermometer with a temperature range from 40°C to 120°C. The deviation of the reference and the measured values of thermocouples increased with temperature. The maximum deviation of a thermocouple was estimated as ± 0.3 K when calibrated for temperatures above 90°C. As mentioned above, the thermocouples were used to measure the heater wall temperature and the liquid temperature at the inlet and outlet of the test section. The fluctuations in temperature reading for each test run were noticed and all these data points were averaged. Thus, the total uncertainties of the liquid temperature at the inlet and outlet of the test section were ± 0.58 K and ± 0.54 K, respectively. Only one thermocouple was used to measure the heater wall temperature. Hence, it can be seen as an area- and time-averaged wall temperature. The measured wall temperature for low flow velocity was compared against the correlations for wall temperature calculation [34, 35] and a deviation of ± 0.63 K was found. Due to the uncertainty in single measurement the total uncertainty for the wall temperature measurement is ± 0.70 K. The uncertainty of the flow rate measurement is ± 1.70%. This uncertainty may arise from small fluctuations of the fluid flow caused by the different components of the loop and particularly the flow meter. In the heat flux measurement of the test heaters, heat losses cause uncertainty. The possible sources of uncertainties in the heat flux (q'') calculation are the power supply (± 0.50%), the fluctuations in measuring the power (± 1.55%), the extended heater surface area (± 4.80%), the long connecting cables and connections (± 5%). The heat loss occurs due to the dissipation of heat to the environment through the insulating materials (3%). All these uncertainties were considered in the heat flux calculation and are given in Table 1. Parameters, such as bubble diameter, bubble base diameter and center of mass position we ensemble-

averaged for many single bubbles (typically 25). According to the so-called three-sigma rule, 68.27% of the captured curves of the bubble ebullition cycles were one standard deviation away from the averaged values and one standard deviation was ± 0.0458 mm. For the sake of clarity, the following graphs just represent the exemplary curves.

3. Results and discussions

In this section, the typical bubble life cycles for different bulk liquid velocities (0.052 m/s and 0.183 m/s) which are captured by the high speed video camera are shown (sub-section 3.1). This section also describes the detailed experimental results of the study on the mutual effect of heater surface wettability, roughness and bulk liquid velocity on the bubble dynamics (sub-section 3.2) and bubble departure (sub-section 3.3) for nucleate boiling.

3.1 Typical bubble life cycle

Figs. 5 (a, b) shows the snapshots of the bubble ebullition cycles, captured by a high-speed video camera for 2 different liquid velocity (0.052 m/s, 0.183 m/s) on a low-wetting polished surface (Sq = 0.01 µm, θ_{hys} = 65.3°). Our imaging technique had sufficient resolution to record the each major stage of a bubble life cycle. It includes bubble generation (i), growth (ii), departure (iii), sliding (iv), lift-off or detachment (v) and the consecutive bubble generation from the same cavity (vi). The corresponding time period for each steps are showed in milliseconds on the images of Figs. 5 (a, b). We see that the bubble diameter and the departure period decrease with the increase of the bulk liquid velocity. On the other hand, the bubble waiting period is much longer for the higher bulk liquid velocity.

3.2 Effect of heater surface characteristics and bulk liquid velocity on the bubble dynamics

This sub-section reports the mutual effect of heater surface characteristics and bulk liquid velocity on the temporal evolution of the bubble equivalent diameter (D_{eq}), bubble base diameter (d_w) and center of mass in y-direction (y_{cm}). The results are presented for a range of bulk liquid velocity (0.052 – 0.183 m/s (approx.)) with three different heater surface characteristics (Sq = 0.01 µm, θ_{hys} = 65.30°; Sq = 0.218 µm, θ_{hys} = 61.47° and Sq = 0.549 µm, θ_{hys} = 58.47°) and heat flux (39.41 - 45.47 kW/m²) in Figs. 6-8. The general findings are that bubble equivalent diameters and departing bubble

diameters are larger for lower bulk liquid velocity (Figs. 6 a, 7 a and 8 a). Not only the bubble equivalent diameter but also the bubble growth rate is faster for lower bulk liquid velocity. Higher bulk liquid velocity reduces the bubble base diameter for a low-wetting smooth surface (Fig. 6 b). A contraction effect at the bubble bases is noticed at the moment of bubble departure for this surface (θ_{hys} = 65.30°) when the bulk liquid velocities are between 0.052 m/s and 0.183 m/s. If the bulk liquid velocity is increased more (0.255 m/s), the bubble base expands during departure (Fig. 6 b) and the bubble moves a comparatively smaller distance along the flow direction prior to departure (Fig. 6 c). Fig. 7 b shows that the bubble base diameter is found to be negatively correlated with the bulk liquid velocity (0.052- 0.12 m/s) for a rough surface (Sq = 0.218 μm, θ_{hys} = 61.47°). The expansion rates of bubble base diameters for another rough surface (Sq = 0.549 μm, θ_{hys} = 58.47°) are almost equal until 2 ms of their growth period at different bulk liquid velocities (Fig. 8 b). After 2 ms, the bubble base experiences contraction and expansion effects. Hence this surface (Sq = 0.549 μm, θ_{hys} = 58.47°) does not show distinguishable correlations between the bulk liquid velocity and the bubble base diameter (Fig. 8 b).

The bulk liquid velocities are found to be positively correlated with the moving distance of center of mass prior to departure for the surface with Sq = 0.218 μm (Fig. 7 c). Fig. 7 (c) further shows that until 5 ms of the bubble growth, the bubble movement in the upward direction is faster for higher bulk liquid velocity. The center of mass of bubbles (Fig. 7 c) for the rough surface (Sq = 0.549 μm, θ_{hys} = 58.47°) does not show a correlation with the bulk liquid velocities. Bubble departure periods are found inversely correlated with the bulk liquid velocity for Sq = 0.01 μm and 0.218 μm. For Sq = 0.549 μm, though the difference between the bubble departure periods for a range of bulk liquid velocity (0.052 m/s-0.183 m/s) is comparatively small (4 ms-5.6 ms), still the bubble departure period is positively correlated with the bulk liquid velocity (Fig. 8 c).

The bubble growth rate, from the view of the heat transfer, has been discussed here. Different heat transfer processes, namely the microlayer evaporation, the heat diffusion through the bubble surface and the condensation heat transfer contribute in the growth of a bubble. A previous article [27] of our group showed that the heater surface characteristics has non-linear relationship with the microlayer evaporation and the bubble growth. It was found that the bubble growth rate is the maximum for an intermediate roughness. This section also shows that the bubble growth rate is maximum for Sq = 0.218 μm compare to Sq = 0.01 μm and 0.549 μm. Figs. 6 a, 7 a and 8 a show that the bulk liquid velocity impacts the bubble growth rate even in the initial growth period (< 2 ms).

Jung and Kim [36] found that the velocity of the microlayer boundary increases with the bubble growth rate. Hence, the bulk liquid velocity may also have influence on the microlayer evaporation. It implies that the microlayer area is positively correlated with the bubble growth rate and negatively correlated with the bulk liquid velocity. The contribution of the heat diffusion through the bubble surfaces reduce with the increase of the bulk liquid velocity, because $Re \propto Nu \propto 1/\delta_w$. On the other hand, the heat transfer coefficient of condensation is greater for the higher liquid velocity as $Nu_c \propto h_c$.

3.3 Effect of heater surface characteristics and bulk liquid velocity on the bubble departure

It was already indicated in the previous sub-section that the bubble departure diameter decreases with the increase of bulk liquid velocity. Sugrue et al. [2] and Rousselet [20] also found similar influence of bulk liquid velocity on the bubble departure diameter. Bubble departure diameters for different heater surfaces are plotted with respect to the bulk liquid velocity for the heat flux range of 42.44 ~ 45.47 kW/m² in Fig. 9. The dash-dot thick trend line represents the average of measured bubble departure diameters for each surface. It shows that in spite of the effect of heater surface characteristics, the bubble departure diameter decreases while the bulk liquid velocity increases. The impact of liquid velocity on the bubble departure diameters is less at high bulk liquid velocity (0.183 - 0.255 m/s). Bubble diameters are more scattered at a bulk liquid velocity from 0.052 to 0.105 m/s compared to a velocity from 0.105 to 0.255 m/s as depicted in Fig. 9. It proves that the significance of the heater surface characteristics for the bubble departure diameter reduces with the increase of the bulk liquid velocity.

Fig. 10 shows the effect of heater surface wettability on the bubble departure diameter (D_d). In general, the bubble departure diameter has been found to increase with the liquid contact angle hysteresis (θ_{hys}) from 42.32° to 65.30° for a range of bulk liquid velocities and heat fluxes. Bubble departure diameters for a heat flux from 39.41 to 45.47 kW/m² and bulk liquid velocity from 0.052 to 0.183 m/s of a particular liquid contact angle hysteresis were averaged. A trend line of the averaged bubble departure diameters is shown in Fig. 10. It shows that the averaged bubble departure diameter increases from 0.75 to 1.70 mm while the liquid contact angle hysteresis increases from 42.32° to 65.30°. A closer look on Fig. 10 shows that the slope of the trend line is stronger for θ_{hys} between 49.22° and 65.30° than that from 49.22° to 42.32°. One of the main reasons for an increase of D_d

with θ_{hys} is that the forces which hinder the bubble departure are greater for low-wetting surfaces [18].

Fig. 11 includes the bubble departure diameters for a heat flux of 39.41 to 45.47 kW/m² and bulk liquid velocity of 0.052 to 0.183 m/s. All these bubble departure diameters are shown by symbols and are averaged here with respect to the root mean square roughness of the surface (*Sq*). A B-spline curve is provided as a trend line (dash-dot thick line). The line shows that the bubble departure diameter increases from the polished surfaces to the surfaces with *Sq* = 0.218 μm. Then it decreases with the increase of surface roughness until *Sq* = 0.549 μm. Bubble departure diameters are found greater for intermediate surface roughness (approximately, *Sq* = 0.108 - 0.218 μm). It should also be underlined here that the impact of heater surface characteristics on the bubble departure dynamics can be both impeding and promoting at different bulk liquid velocities. Next section analyzes these phenomena.

4. Theoretical analysis of bubble departure

4.1 Analysis of important parameters

While a nucleated bubble grows on a vertical heater surface, several forces at the liquid-vapor and vapor-solid interfaces come into play. The literature review in section 1 summarizes that buoyancy (F_b), surface tension (F_s), unsteady drag (F_{du}), quasi-steady drag (F_{qs}) and additional added-mass force ($F_{growth,bulk}$) are the dominant forces for the bubble departure. The expressions of the forces consist of basic parameters, such as physical properties of the fluid (ρ_l, ρ_g, σ, v), slip velocity of the bubble ($\Delta V = V_l - V_b$) and geometrical parameters of the bubble (d_w, R, α, β, φ).

Table 2 recapitulates these forces and parameters. The bubble inclination φ angle is included in the equation for unsteady forces. Though the contact angles (α, β) are expected to vary with the expansion and contraction of the bubble base, some groups considered the bubble contact angles as constant ($\alpha = 45°$, $\beta = 36°$ [13]). Measuring the time dependent bubble contact angle is complicated, especially at flow boiling conditions. Therefore, the influence of bulk liquid velocity on the bubble contact angles (α, β) is not fully conclusive until now. The present experiments were performed at atmospheric pressure and low subcooling. Hence, the experimental boundary conditions do not alter

the fluid properties much. Thus, it can be assumed that the total sum of the forces changes with the temporal evolution of geometrical parameters of bubbles.

The experimental results show that the bubble departure diameter is greater for a larger bubble base diameter (d_w). Further, d_w is an important parameter in calculating F_s, F_{cp} and F_h. Among them, F_s is recommended by many groups as a significant force that holds the bubble on the surface. Moreover, F_b is greater for larger bubbles, as $F_b \propto R^3$. On that account, these two geometric parameters (R, d_w) of a bubble play an opposite role in the bubble departure process. According to Klausner et al. [13], unsteady drag force (F_{du}) acts towards the heater surface and Thorncroft et al. [11] suggested that additional added mass force ($F_{growth,bulk}$) solely acts upward and expedites the bubble departure process. The directions of these forces (F_{du}, $F_{growth,bulk}$) were already introduced in Fig. 2. The bubble radius (R) and the bubble growth rate ($\dot{R}$), which are geometric parameters, are both factors of F_{du} and $F_{growth,bulk}$. $F_{growth,bulk}$ is dependent on bulk liquid velocity (V_l) and F_{qs} is affected by relative velocity ($\Delta V = V_l$-V_b). As a result, the bubble departure can be predicted by the bubble radius (R), bubble base diameter (d_w), bubble growth rate ($\dot{R}$ *or* dR/dt) and relative velocity (ΔV=V_l-V_b). F_b and $F_{growth,bulk}$ increase largely over time for a growing bubble and they contribute a huge amount to overcome the hindering exerted on a bubble by F_s, F_{duy} and F_{qs} during departure. F_b, $F_{growth,bulk}$ *and* F_{duy} are third and second degree functions of bubble radius. It implies that the bubble size (R) and bubble growth rate (dR/dt) play a significant role for bubble departure. The bubble departure for different of heater surface wetting characteristics and roughness is analyzed below based on bubble size (D_{eq}), base diameter (d_w), bubble growth rate (dR/dt) and relative velocity (V_l-V_b) (Figs. 12 and 13).

Fig. 12 shows that bubble size (D_{eq}), bubble base diameter (d_w) and bubble growth rate (dR/dt) increase with the liquid contact angle hysteresis. The effect of surface wettability on the relative velocity before bubble departure and on the bubble growth rate seems opposite to each other. However, surface tension force (F_s) and unsteady drag force (F_{duy}) on a bubble can be greater for low-wetting surfaces, since D_{eq}, d_w and dR/dt are greater for a surface with higher liquid contact angle hysteresis. Both of these forces retard the bubble departure. A large bubble size for a low-wetting surface also leads to a greater buoyancy force (F_b). Additional-added mass force ($F_{growth,bulk}$) and quasi-steady drag force (F_{qs}) may become greater with the decrease of surface wettability and expedite the bubble departure process. Fig. 12 manifests that the bubble departure is comparatively

earlier and a bubble departure diameter is smaller for well-wetting surfaces. It means that the geometrical parameters are comparatively less effective for low-wetting surfaces compared to well-wetting surfaces in the bubble departure

The influence of surface roughness on the dominant parameters of bubble departure is shown in Fig. 13. Bubble size (D_{eq}) and bubble base diameter (d_w) are larger for the intermediate roughness of Sq = 0.218 μm. A relative velocity ($\Delta V = V_l - V_b$) is generally lower for Sq = 0.108 μm and it exceeds 0.12 m/s during departure. A common tendency of the temporal evolutions of bubble growth rate (dR/dt) is that they become almost asymptotic at bubble departure. The bubble growth rate is lower for Sq = 0.549 μm compared to the other two rough surfaces. The bubble departure diameter is slightly smaller for Sq = 0.108 μm than for Sq = 0.218 μm, though the departure period is much smaller for the former surface (Sq = 0.108 μm) compared to the latter (Sq = 0.218 μm).

Fig. 13 shows that the bubble departure periods are longer for larger bubble bases. Similar results can be found in Fig. 12. Since the effect of bubble growth rate is indistinguishable for Sq = 0.108 μm and 0.218 μm, (Fig. 13), buoyancy (F_b) and additional added mass force ($F_{growth,bulk}$) must be convincingly greater for surfaces with Sq = 0.108 μm. Surface tension force (F_s) towards the heater wall is expected to be lower for Sq = 0.108 μm and greater for Sq = 0.218 μm due to the smaller and larger bubble base diameter, respectively. The unsteady drag force (F_{du}) may be higher due to the larger bubble size at Sq = 0.218 μm. The low-wetting surface (θ_{hys} = 65.30°) in Fig. 12 and the surface with the roughness of Sq = 0.218 μm in Fig. 13 were found to produce a larger bubble departure diameter and a longer departure period. Thus, the behaviour of these two surfaces is similar with respect to bubble departure size and period.

The non-zero d_w at bubble departure leads to the conclusion, that surface tension force (F_s) keeps acting during departure. At such a condition, a bubble departs from the cavity, slides, but does not detach from the surface. Hence, the departure mechanism for the bubbles in Figs. 12 and 13 shall be sliding rather than detachment. All the considered geometrical parameters of a bubble do not account for the actual magnitude of forces. But they represent the qualitative implications of the associated forces. Bubble size (R) and the bubble growth rates ($\dot{R}$) are repetitively used in models for both the hindering and expediting forces for bubble departure. That is, some geometrical parameters have a counteracting effect on bubble departure. As a consequence, estimating the bubble departure by a

single bubble geometrical parameter would not be sufficient. Hence, a proportional representation of these geometrical parameters may provide a criterion for the bubble departure.

4.2 Formulation of a bubble departure criterion

The derivation of a bubble departure criterion based on geometrical parameters is not uncommon in literature. Wu et al. [28] assumed that the effect of bubble contact angle is insignificant for bubble departure and the surface tension force is proportional to the bubble base diameter. With this assumption, they proposed a simple bubble departure criterion ($V_l \cdot R$= constant) that comprises the bulk liquid velocity and the bubble size. Such an approach is improved further in the present work with further considerations. As already discussed above, the buoyancy force (F_b) acts along the flow direction and promotes bubble departure. R_{eq}^3 is the main factor in the expression of buoyancy force (F_b). If the effect of bubble contact angle is neglected, then surface tension force (F_s) is mainly a function of d_w. The surface tension force (F_s) impedes the departure of a bubble as it acts towards the heater surface. One proportional term (d_w/R_{eq}^3) can be formulated out of these two forces. The proposed term represents the dominating characteristics of the ratio of surface tension (F_s) and buoyancy (F_b) forces. Apart from the buoyancy and surface tension force, three other forces (F_{du}, $F_{growth,bulk}$ and F_{qs}) are considered as being influential for bubble departure. Among them, F_{du} and $F_{growth,bulk}$ act in reverse directions and both of them are function of the bubble growth rate ($\dot{R}$). The role of F_{qs} in the departure of a bubble is dependent on the (+ or -) sign of the relative velocity ($\Delta V = V_l - V_b$). Considering the last three forces, another term as a function of bubble growth rate ($\dot{R}$) and relative velocity ($V_l - V_b$) is suggested here. Hence, it is postulated that these terms decrease with time and they become asymptotic when a bubble departs from its nucleation cavity. This means, that unlike the bubble size, the importance of the bubble base diameter in the term (d_w/R_{eq}^3) reduces over time. Another term was a function of $\dot{R}$ and ($V_l - V_b$). As both of these terms become asymptotic, their time derivative is multiplied to find the minimum value. The relation then becomes as follows:

$$min\left\{\frac{d}{dt}\left(\frac{d_w}{R_{eq}^3}\right)\cdot\frac{d}{dt}\left[\, f\left(\dot{R}, V_l - V_b\right)\right]\right\}. \qquad (2\text{ a})$$

This is proposed as a bubble departure criterion, i.e., a bubble departs from a nucleation cavity when it satisfies Eqn. 2 a. The experimental data of the present study were used to propose a function

$f(\dot{R}\cdot(V_l\text{-}V_b))$. For that we considered the following options: $\dot{R}(V_l\text{-}V_b)$, $\dot{R}^2(V_l\text{-}V_b)$, $\dot{R}/(V_l\text{-}V_b)$ and $\dot{R}^2/(V_l\text{-}V_b)$. The bubble diameters which agree with the proposed expression (Eqn. 2 a), have been compared against the experimental results. From that is it found, that the numerically obtained bubble diameters fit best against the experimental result for the following criterion:

$$min\left\{\frac{d}{dt}\left(\frac{d_w}{R_{eq}^3}\right)\cdot\frac{d}{dt}\left[\dot{R}_{eq}^2\left(V_l-V_b\right)\right]\right\}. \qquad (2\text{ b})$$

The comparison of the modelled and measured bubble departure diameters is shown in Fig. 14. The experimentally measured bubble departure diameters for all the heater surfaces and bulk liquid velocities for upward flow boiling are plotted along the x-axis of Fig. 14. The y-axis represents the diameter of the bubbles obtained from Eqn. 2 b. 66% of the experimentally measured bubble departure diameters satisfy the proposed criterion with ±10% deviation. 90% are within a ±25% of error bound.

5. Conclusion

In the present study, we performed a thorough investigation on the influence of heater surface characteristics and bulk liquid velocity on the departure dynamics of the isolated bubble during nucleate boiling. We performed experiments using 9 different surfaces (θ_{hys} = 42.32° - 68.56°, Sq = 0.01- 0.55 μm) for a range of bulk liquid velocity from 0.052 to 0.183 m/s and the heat fluxes of 39.41 to 45.47 kW/m². The experiments were conducted at atmospheric pressure with degassed-deionized water at low-subcooling (1.9 ± 0.25 K) and the material of the test heaters was stainless steel. High-resolution imaging technique was used to record the bubble life cycle. We may summarize the experimental findings as follows:

i) Bubble departure diameters decrease with the increase of bulk liquid velocity for all heater surface characteristics. From averaged bubble departure diameters it was found that the decrease of bubble departure diameter is greater for low bulk liquid velocity regime (0.052 - 0.16 m/s).

ii) The bubble departure diameters were found to increase from 0.75 mm to 1.75 mm with the increase of liquid contact angle hysteresis from 42.32° to 65.30°.

iii) The bubble growth rates were found largest for an intermediate roughness of *Sq* between 0.108 and 0.218 μm considering a range of bulk liquid velocity and heat flux. Larger bubble departure diameters are obtained for surfaces with *Sq* = 0.218 μm.

iv) Finally, a bubble departure criterion was derived. 90% of the experimental bubble departure diameters satisfy this criterion with ± 25% errors.

The outcome of this study may help to improve the numerical model to predict the bubble departure diameter. The results provide further useful insights for designing the heat transfer surfaces.

Acknowledgments

This study acknowledges the contribution of Dr. Ralf Helbig and Dr. Astrid Drechsler of IPFDD for allowing the authors to use the goniometer in their laboratory. The authors like to thank Dr.-Ing. Clemens Schneider of IPM, Hochschule Zittau/Görlitz and Dipl.-Ing. Thomas Geißler of Sunfire GmbH for their supports in the experiment.

Conflict of interest

There is no conflict of interests.

References

[1] S. Moghaddam, K. Kiger, Physical mechanisms of heat transfer during single bubble nucleate boiling of FC-72 under saturation conditions-I. Experimental investigation. International Journal of Heat and Mass Transfer, 2009. **52**: p. 1284-1294.

[2] R. Sugrue, J.B., T. McKrell, An experimental study of bubble departure diameter in subcooled flow boiling including the effects of orientation angle, subcooling, mass flux, heat flux and pressure. Nuclear Engineering and Design, 2014. **279**: p. 182-188.

[3] A. Zou, D. P. Singh, S. C. Maroo, Early evaporation of microlayer for boiling heat transfer enhancement. Langmuir, 2016. **32**: p. 10808-10814.

[4] S. H. Kim, G. C. Lee, J. Y. Kang, K. Moriyama, H. S. Park, M. H. Kim, A study of nucleate bubble growth on microstructured surface through high speed and infrared visualization. International Journal of Multiphase Flow, 2017. **95**: p. 12-21.

[5] R. Sugrue, J. Buongiorno, A modified force-balance model for prediction of bubble departure diameter in subcooled flow boiling. Nuclear Engineering and Design, 2016. **305**: p. 717-722.

[6] G. Sateesh, S. K. Das, A. R. Balakrishnan, Analysis of pool boiling heat transfer: effect of bubbles sliding on the heating surface. International Journal of Heat and Mass Transfer, 2005. **48**: p. 1543-1553.

[7] C. Gerardi, J. Buongiorno, L.W. Hu, T. McKrell, Study of bubble growth in water pool boiling through synchronized, infrared thermometry and high-speed video. International Journal of Heat and Mass Transfer, 2010. **53**: p. 4185-4192.

[8] M. A. Amidu, S. Jung, H. Kim, Direct experiment measurement for partitioning of wall heat fluy during subcooled flow boiling: Effect of bubble areas of influence factor. International Journal of Heat and Mass Transfer, 2018. **127**: p. 515-533.

[9] S.B. Jung, H.D. Kim, An experimental method to simultaneously measure the dynamics and heat transfer associated with a single bubble during nucleate boiling on a horizontal surface. International Journal of Heat and Mass Transfer, 2014. **73**: p. 365-375.

[10] W. Ding, E. Krepper, U. Hampel, Evaluation of the microlayer contribution to bubble growth in horizontal pool boiling with a mechanistic model that considers dynamic contact angle and base expansion. International Journal of Heat and Fluid Flow, 2018. **72**: p. 274-287.

[11] G. E. Thorncroft, J. F. Klausner, R. Mei, Bubble forces and detachment models. Multiphase Science and Technology, 2001. **13**: p. 35-76.

[12] S. Raj, M. Pathak, M. K. Khan, An analytical model for predicting growth rate and departure diameter of a bubble in subcooled flow boiling. International Journal of Heat and Mass Transfer, 2017. **109**: p. 470-481.

[13] J. F. Klausner, R. Mei, D. M. Bernhard, L. Z. Zeng, Vapor bubble departure in forced convection boiling. International Journal of Heat and Mass Transfer, 1993. **36**: p. 651-662.

[14] B. J. Yun, A. Splawski, S. Lo, C.H. Song, Prediction of a subcooled boiling flow with advanced two-phase flow models. Nuclear Engineering Design, 2012. **253**: p. 351-359.

[15] Y.P. Chang, Some possible critical conditions in nuleate boiling. Journal of Heat Transfer, 1963. **85**: p. 89-100.

[16] Y.J. Cho, S.B. Yum, J.H. Lee, G.C.Park, Development of bubble departure and lift-off diameter models in low heat flux and low flow velocity conditions. International Journal of Heat and Mass Transfer, 2011. **54**: p. 3234-3244.

[17] H. T. Phan, N. Caney, P. Marty, S. Colasson, J. Gavillet, Surface wettability control by nanocoating: The effects on pool boiling heat transfer and nucleation mechanism. International Journal of Heat and Mass Transfer, 2009. **52**: p. 5459-5471.

[18] Y. Nam, J. Wu, G. Warrier, Y.S. Ju Experimental and numerical study of single bubble dynamics on a hydrophobic surface. Journal of Heat Transfer, 2009. **131**: p. 1-7.

[19] Y. Nam, E. Aktinol, V.K. Dhir, Y. S. Ju, Single bubble dynamics on a superhydrophilic surface with artificial nucleation sites. International Journal of Heat and Mass Transfer, 2011. **54**: p. 1572-1577.

[20] Y. L. Rousselet, Interacting effects of inertia and gravity on bubble dynamics, in Mechanical Engineering. 2014, University of California.

[21] Z. Sun, X. Chen,, H. Qiu, Bubble dynamics and heat transfer during pool boiling on wettability patterned surfaces. Heat Transfer Engineering, 2018. **39**: p. 663-671.

[22] D. Sarker, R. Franz, W. Ding, U. Hampel, Single bubble dynamics during subcooled nucleate boiling on a vertical heater surface: An experimental analysis of the effects of surface characteristics. International Journal of Heat and Mass Transfer, 2017. **109**: p. 907-921.

[23] P. Goel, A. K. Nayak, P. P. Kulkarni, J. B. Joshi, Experimental study on bubble departure characteristics in subcooled nucleate pool boiling. International Journal of Multiphase Flow, 2017. **89**: p. 163-176.

[24] D. Sarker, W. Ding, R. Franz, O. Varlamova, P. Kovats, K. Zähringer, U. Hampel, Investigations on the effects of heater surface characteristics on the bubble waiting period during nucleate boiling at low subcooling. Experimental Thermal and Fluid Science, 2019. **101**: p. 76-86.

[25] H.J. Jo, S.H. Kim, H. Kim, M. H. Kim, Nucleate boiling performance on nano/microstructures with different wetting surfaces. Nanoscale Research Letters, 2012. **7**.

[26] C.M. Kruse, T. Anderson, C. Wilson, C. Zuhlke, D. Alexander, G. Gogos, S. Ndao, Enhanced pool boiling heat transfer and critical heat flux on femtosecond laser processed stainless steel surfaces. International Journal of Heat and Mass Transfer, 2015. **82**: p. 109-116.

[27] D. Sarker, W. Ding, U. Hampel, Bubble growth during subcooled nucleate boiling on a vertical heater: A mechanistic attempt to evaluate the role of surface characteristics on microlayer evaporation. Applied Thermal Engineering, 2019. **153**: p. 565-574.

[28] W. Wu, P. Chen, B. G. Jones, T. A. Newell, A study on bubble detachment and the impact of heated surface structure in subcooled nucleate boiling flows. Nuclear Engineering and Design, 2008. **238**: p. 2693-2698.

[29] J. Yoo, C. E. Estrada-Perez, Y. A. Hassan, Experimental study of bubble dynamics and wall heat transfer arising from a single nucleation site at subccoled flow boiling conidtions-Part 1: Experimental methods and data quality verification. International Journal of Multiphase Flow, 2016. **84**: p. 315-324.

[30] S. Maity, Effect of velocity and gravity on bubble dynamics, U.o. California, Editor. 2000.

[31] U. Harm, W. Fürbeth, K.-M. Mangold, K. Jüttner, Novel protective coatings for steel based on a combination of self-assembled monolayers and conducting polymers, in Macromolecular Symposia. 2002. p. 65-76.

[32] Y. Yuan, T. R. Lee, Contact angle and wetting properties [Chapter 1]. Surface Science Techniques, 2013.

[33] C. Schneider, R. Hampel, A. Traichel, J. Herold, L. Kirsten, S. Meissner, E. Koch, A. Hurtado. Experimental investigation of Nucleate boiling on optical transparent heated surfaces with optical coherence tomograpgy (OCT) and infrared thermography. in 19th International Conference on Nuclear Engineering. 2011. Chiba, Japan: JSME.

[34] W.H. McAdams, Heat transmission. 1942, New York: McGraw-Hill.

[35] J. C. Chen, Correlation for boiling heat transfer to saturated fluids in convective flow. Industrial and Engineering Chemistry Process Design and Development, 1966. **5**: p. 322-329.

[36] S. Jung, H. Kim, Hydrdynamic formation of a microlayer underneath a boiling bubble. International Journal of Heat and Mass Transfer, 2018. **120**: p. 1229-1240.

Figures:

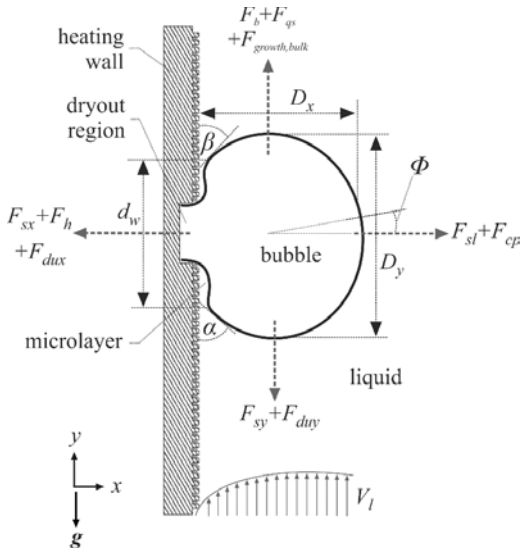

Fig. 1: Forces acting on the bubble during upward flow boiling.

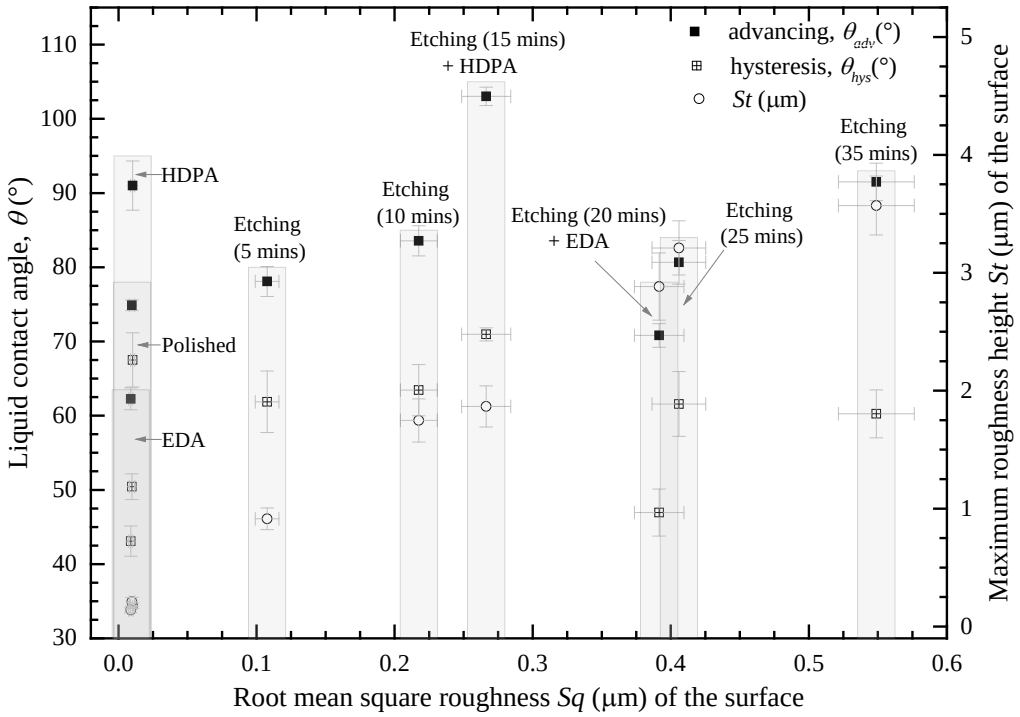

737

738 *Fig. 2: Surface parameters and the corresponding preparation methods of the test samples.*

739

740

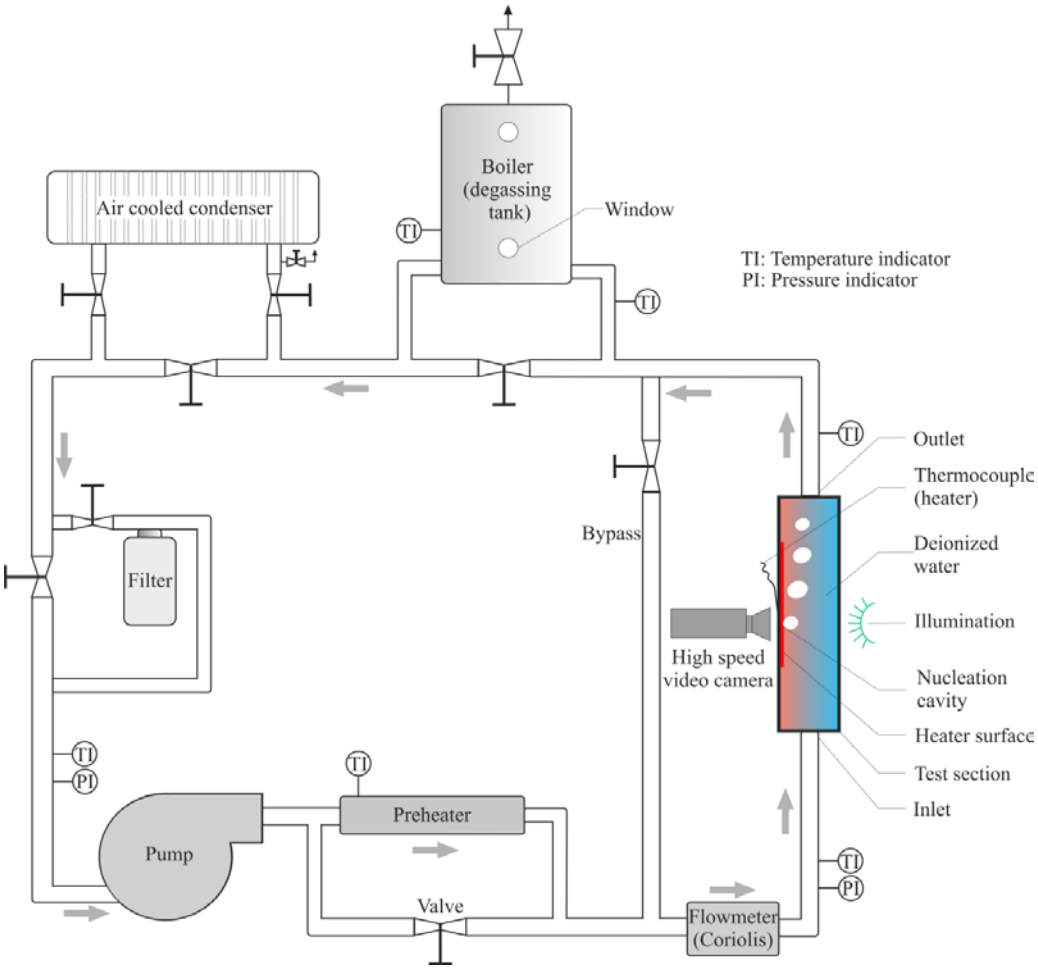

741

742 *Fig. 3. A schematic of the experimental facility.*

743

744

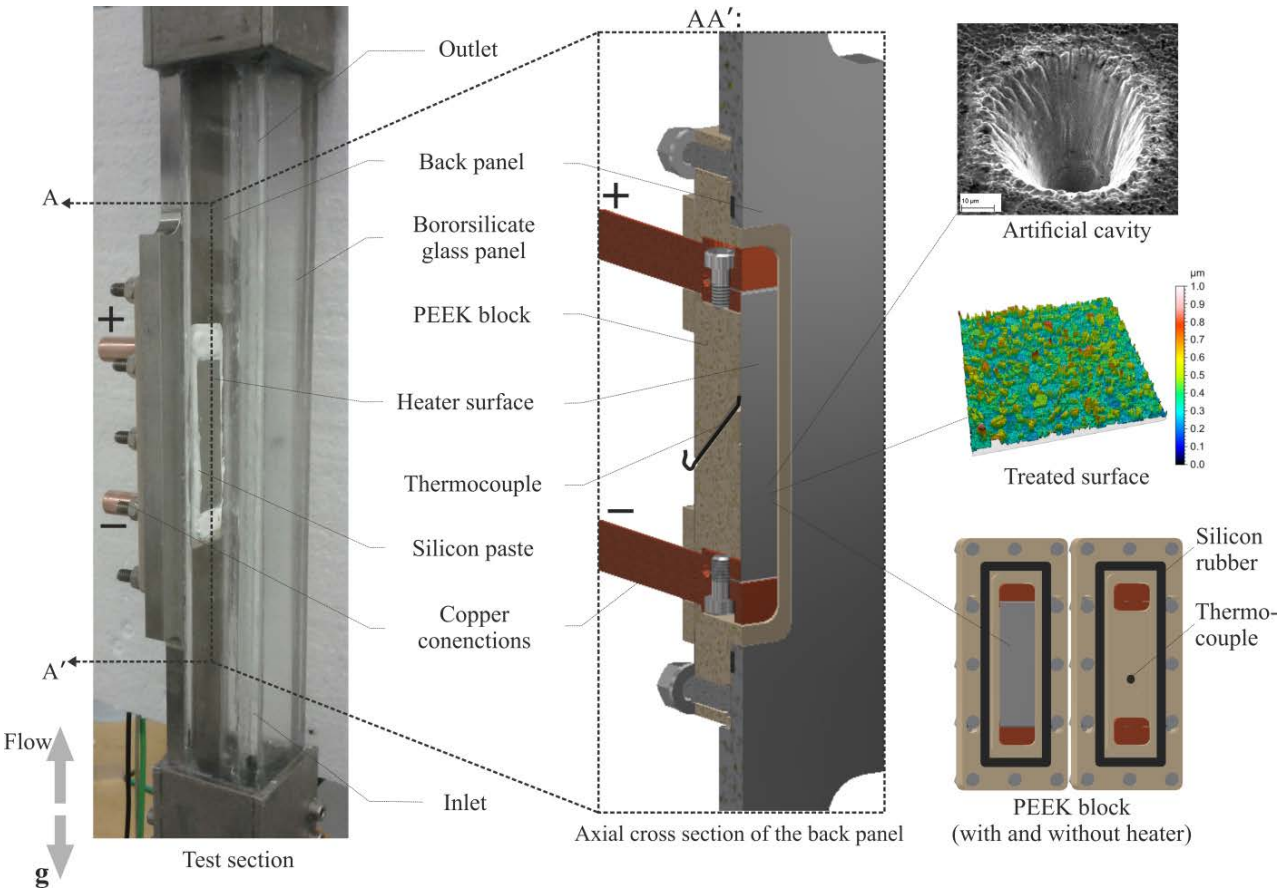

Fig. 4. Details of the test section.

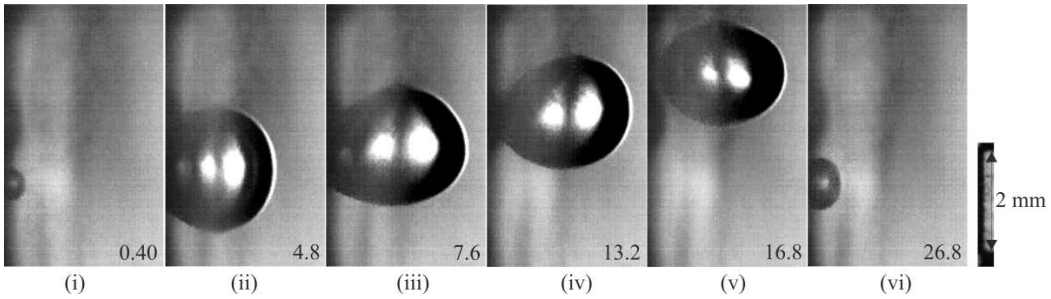

(a)

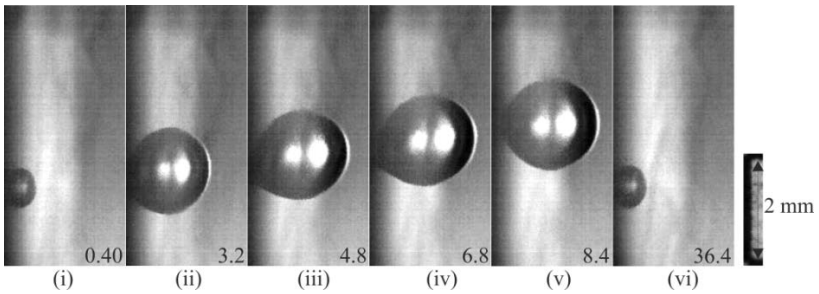

(b)

Fig. 5. Video sequence showing the different stages of a bubble ebullition cycle on Sq = 0.01 μm, θ_{hys} = 65.3° for q'' = 42.44 kW/m², ΔT_w = 9.20 K, ΔT_{sub} = 2.10 K, 0.052 m/s (a), q'' = 42.44 kW/m², ΔT_w = 6.56 K, ΔT_{sub} = 1.72 K, 0.183 m/s (b).

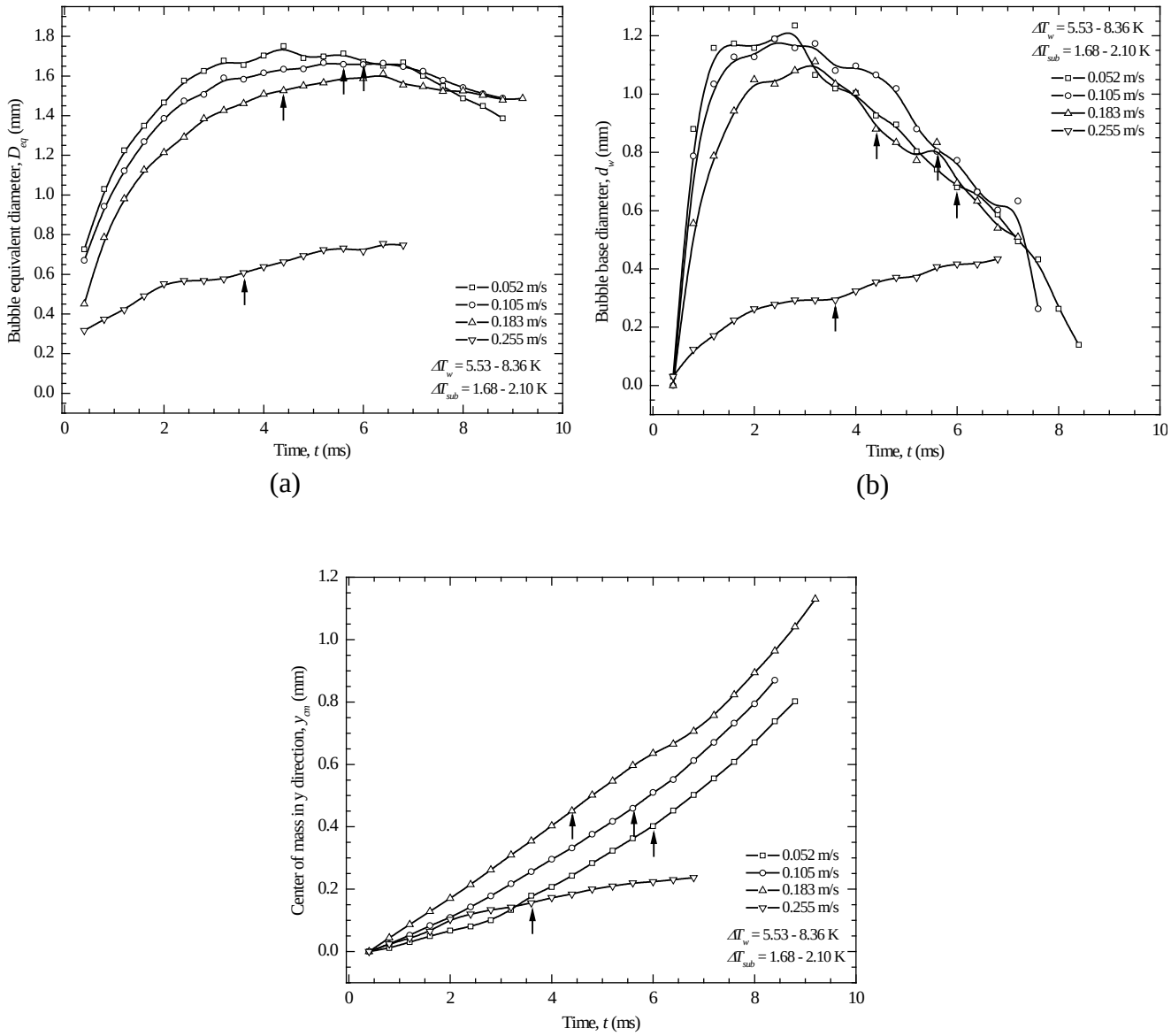

Fig. 6. Bulk liquid velocity effect on the temporal evolution of the bubble equivalent diameter (a), bubble base diameter (b) and center of mass of bubble (c) for Sq = 0.01 μm, θ_{hys} = 65.30° and q″ = 39.41 kW/m². ↑ indicates the bubble departure point.

772

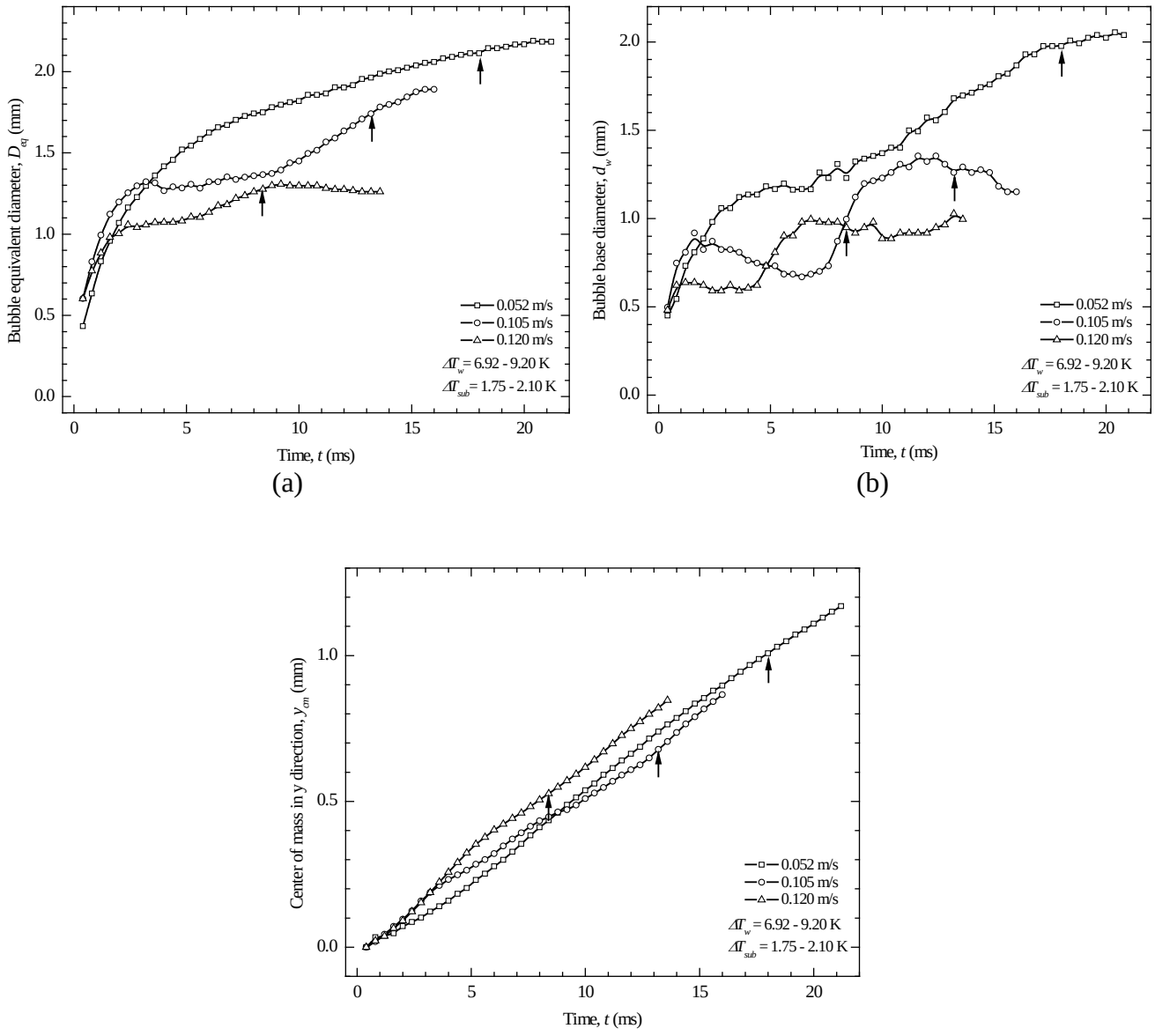

Fig. 7. Bulk liquid velocity effect on the temporal evolution of the bubble equivalent diameter (a), bubble base diameter (b) and center of mass of bubble (c) for Sq = 0.218 μm, θ_{hys} = 61.47° and q″ = 42.44 kW/m². ↑ indicates the bubble departure point.

773

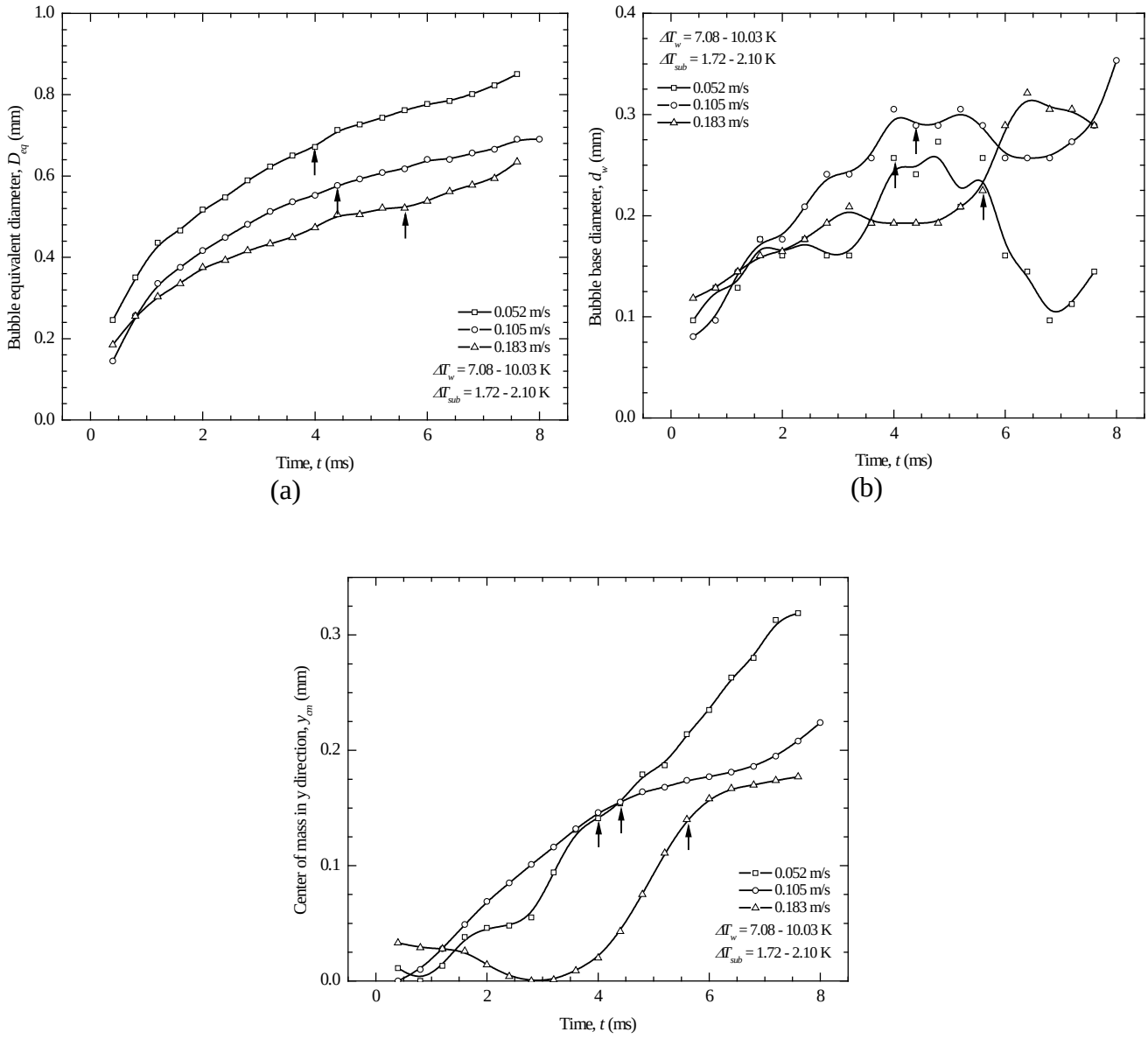

Fig. 8. Bulk liquid velocity effect on the temporal evolution of the bubble equivalent diameter (a), bubble base diameter (b) and center of mass of bubble (c) for Sq = 0.549 μm, θ_{hys} = 58.47° and q″ = 45.47 kW/m². ↑ indicates the bubble departure point.

774

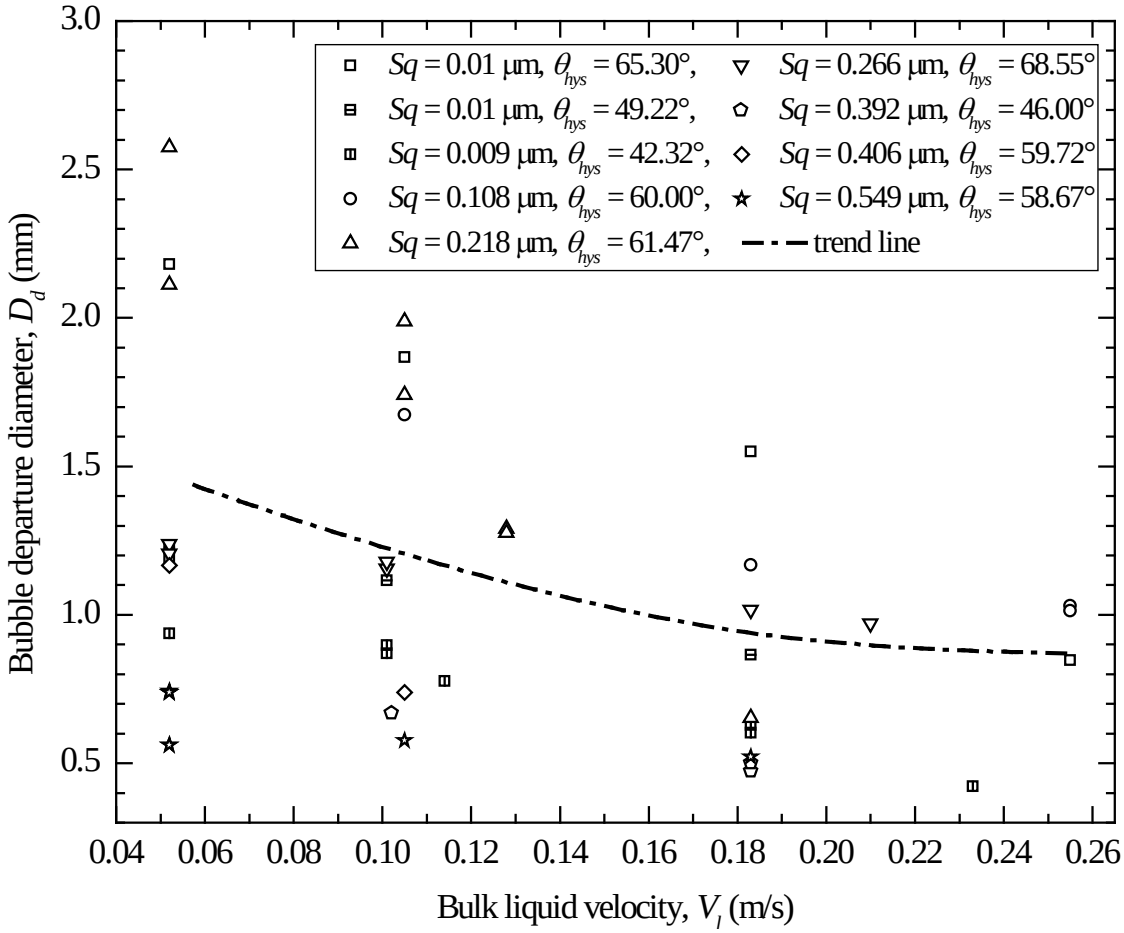

Fig. 9. Effect of bulk liquid velocity on the bubble departure (q'' = 42.44 - 45.47 kW/m², ΔT_w = 6.03 - 10.03 K, ΔT_{sub} = 1.90 ± 0.20 K).

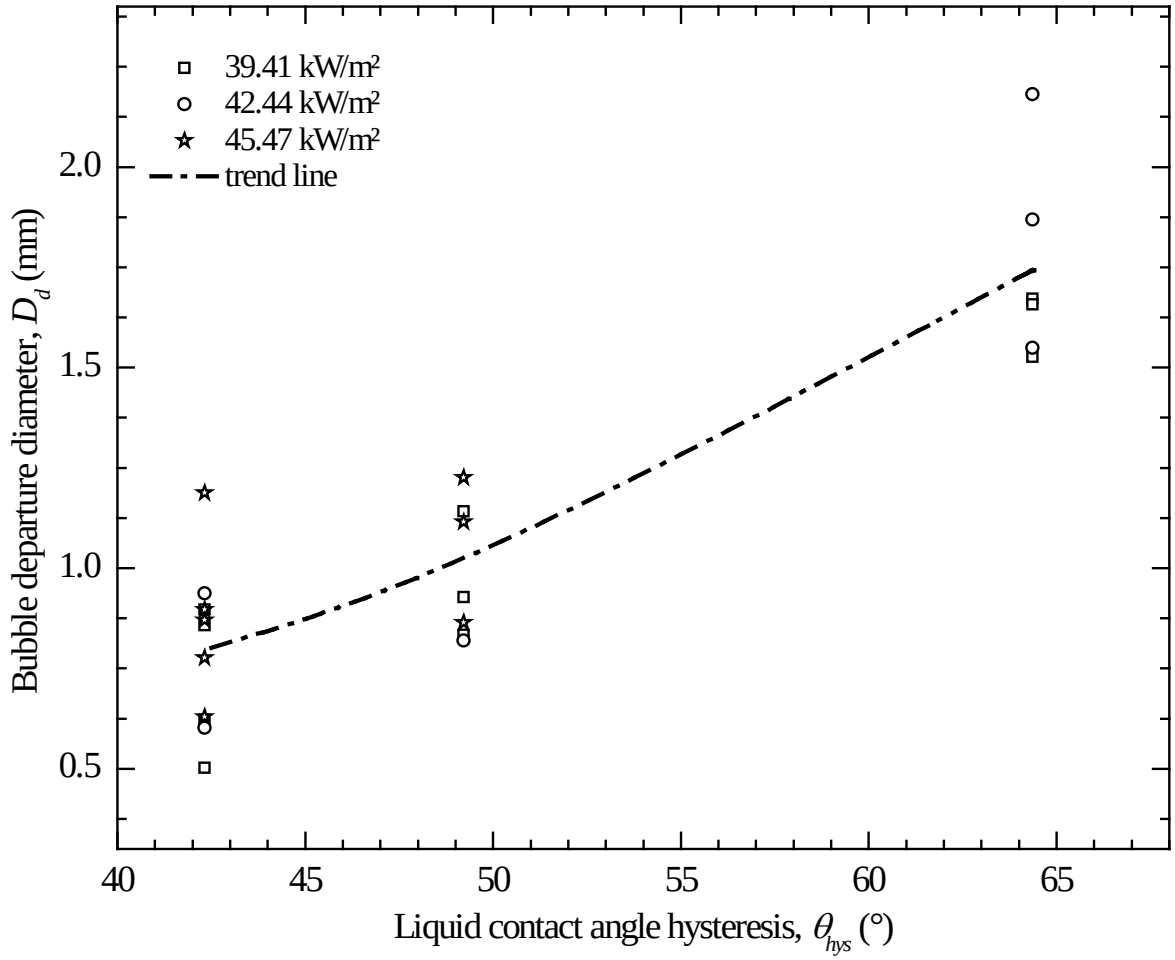

Fig. 10. Effect of heater surface wettability on the bubble departure (ΔT_w = 6.03 - 10.03 K, ΔT_{sub} = 1.90 ± 0.20 K, V_l = 0.052 - 0.183 m/s).

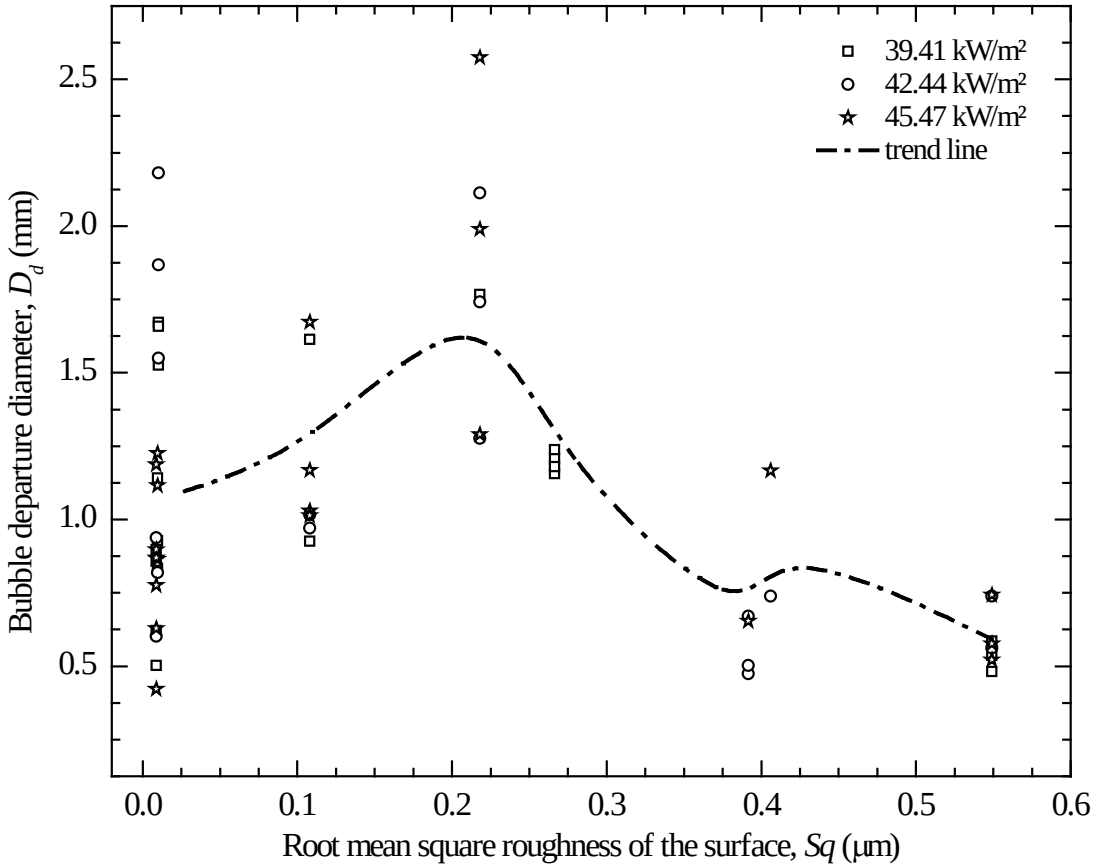

796

797 *Fig. 11. Effect of heater surface roughness on bubble departure diameter (ΔT_w = 6.03 - 10.03 K,*

798 *ΔT_{sub} = 1.90 ± 0.20 K, V_l = 0.052 - 0.183 m/s).*

799

800

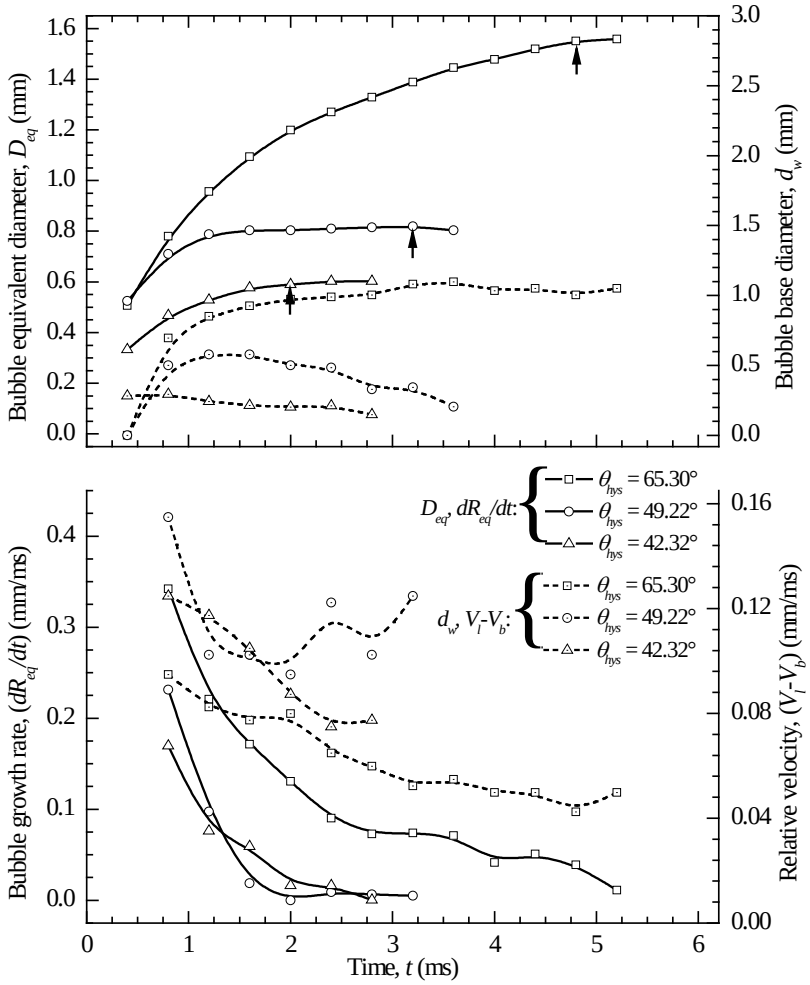

Fig. 12. Effect of influential parameters on the bubble departure for surfaces with different wetting characteristics ($q'' = 42.44$ kW/m², $\Delta T_w = 6.56$ K, $\Delta T_{sub} = 1.72$ K, $V_l = 0.183$ m/s). ↑ indicates the bubble departure point.

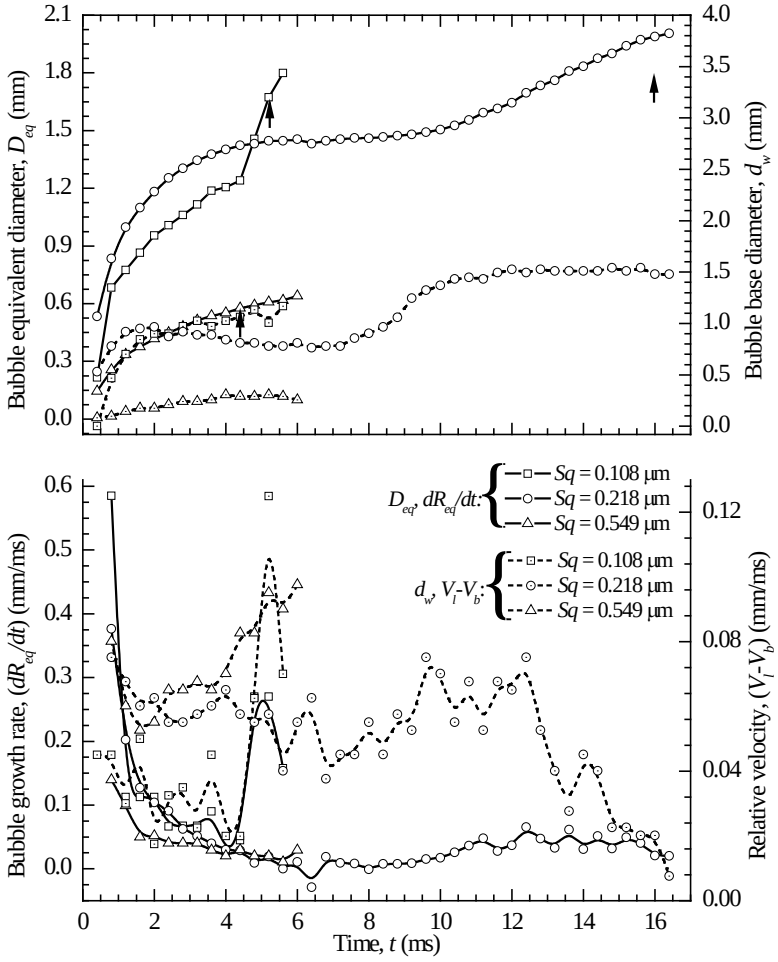

Fig. 13. Effect of influential parameters on the bubble departure for surfaces with different roughness (q'' = 45.47 kW/m², ΔT_w = 8.70 K, ΔT_{sub} = 1.76 K, V_l = 0.105 m/s). ↑ indicates the bubble departure point.

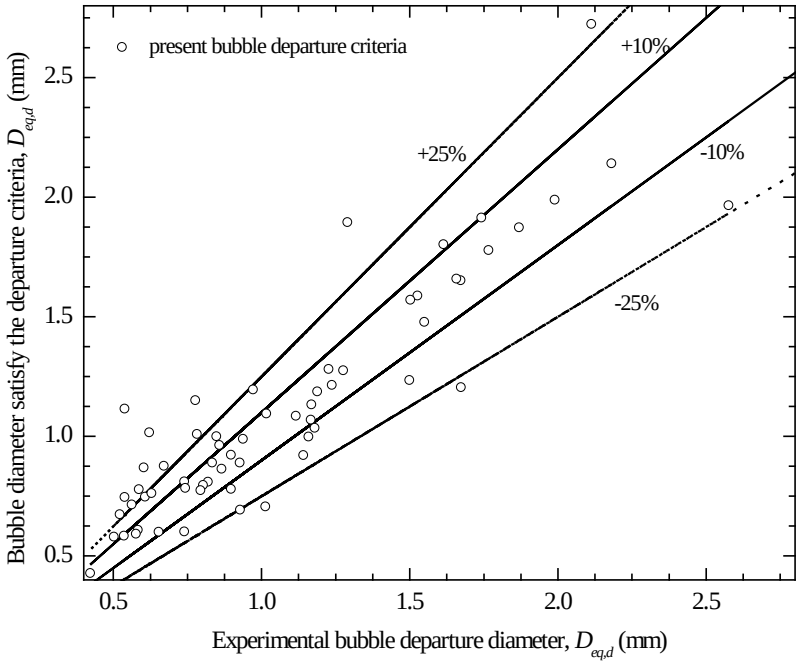

Fig. 14. Comparison of experimental and numerical bubble departure diameter.

Tables:

Table 1: Measurement and calculation uncertainties.

Parameters	Instruments	Locations	Uncertainties		Total uncertainties
			Calibration/static	Measurement	
Temperature	K-type thermocouples	Test section inlet	± 0.50 K	± 0.30 K	± 0.58 K
		Test section outlet	± 0.50 K	± 0.20 K	± 0.54 K
		Heater wall	± 0.30 K	± 0.63 K	± 0.70 K
Flow meter	Coriolis mass flow meter	Test section inlet	± 0.20%	± 1.70%	± 1.71%
Heat flux	Power supply, DAS	Heater wall	± 5.02%	± 5.04%	± 7.12%
Bubble sizes	HSVC				± 40.985 μm

Table 2: Simplified expressions for the forces governing bubble departure [5, 11].

Force	Expression	Simplification
Surface tension force	$F_{sy} = -1.25 d_w \sigma \frac{\pi(\alpha-\beta)}{\pi^2-(\alpha-\beta)^2}(\sin\alpha+\sin\beta).$	$F_s = f(d_w,\alpha,\beta).$
	$F_{sy} = -d_w \sigma \frac{\pi}{(\alpha-\beta)}(\cos\beta-\cos\alpha).$	
Buoyancy force	$F_b = \frac{4}{3}\pi R^3(\rho_l-\rho_g)g.$	$F_b = f(R).$
Unsteady drag force	$F_{duy} = -\rho_l \pi R^2\left(\frac{3}{2}C_s\dot{R}^2 - R\ddot{R}^2\right)\sin\varphi.$	$F_{du} = f(R,\dot{R},\varphi).$
	$F_{dux} = -\rho_l \pi R^2\left(\frac{3}{2}C_s\dot{R}^2 - R\ddot{R}^2\right)\cos\varphi.$	
Quasi-steady drag force	$F_{qs} = 6\pi\nu\rho_l \Delta V R\left[\frac{2}{3}+\left[\left(\frac{12}{Re_b}\right)^{0.65}+0.796^{0.65}\right]^{-1/0.65}\right].$	$F_{qs} = f(\Delta V,R).$
Additional added-mass	$F_{growth,bulk} = 2\pi\rho_l R^2 V_{lx}\dot{R}.$	$F_{growth,bulk} = f(R,\dot{R},V_l).$
Contact pressure force	$F_{cp} = \frac{\pi d_w^2}{4}\frac{2\sigma}{5R}.$	$F_{cp} = f(d_w,R).$
Shear lift force	$F_{sl} = \frac{1}{2}\rho_l \Delta V^2 \pi R^2\left[3.877 G_s^{0.5}\left[Re_b^{-2}+0.014G_s^2\right]^{0.25}\right].$ $C_L = 0.8G_s,\ G_s = \frac{dV}{dx}\frac{R}{\Delta V}.$	$F_{sl} = f(\Delta V,R).$
Hydrodynamic pressure force	$F_h = \frac{9}{8}\rho_l \Delta V^2 \frac{\pi d_w^2}{4}.$	$F_h = f(\Delta V,d_w).$

Appendix

Table 3: Experimental parameters.

Surface parameters				**Heat flux q'' (kW/m²)**	***Bulk liquid velocity V_l (m/s)***	***Subcooling ΔT_{sub} (K)***	***Wall superheat ΔT_w (K)***
Roughness	***Wettability***						
Rms roughness Sq (μm)	***Advancing θ_{adv} (°)***	***Receding θ_{rec} (°)***	***Hysteresis θ_{hys} (°)***				
0.01023	91	25.7	65.3	39.41	0.052	2.1	8.36
0.01023	91	25.7	65.3	39.41	0.105	1.76	7.14
0.01023	91	25.7	65.3	39.41	0.183	1.72	6.03
0.01023	91	25.7	65.3	39.41	0.255	1.68	5.53
0.01023	91	25.7	65.3	42.44	0.052	2.1	9.196
0.01023	91	25.7	65.3	42.44	0.105	1.76	7.924
0.01023	91	25.7	65.3	42.44	0.183	1.72	6.56
0.01023	91	25.7	65.3	42.44	0.255	1.68	6.24
0.00976	74.87	25.65	49.22	39.41	0.052	2.1	8.36
0.00976	74.87	25.65	49.22	39.41	0.105	1.76	7.14
0.00976	74.87	25.65	49.22	39.41	0.183	1.72	6.03
0.00976	74.87	25.65	49.22	42.44	0.183	1.72	6.56
0.00976	74.87	25.65	49.22	45.47	0.052	2.1	10.032
0.00976	74.87	25.65	49.22	45.47	0.105	1.76	8.698
0.00976	74.87	25.65	49.22	45.47	0.183	1.72	7.08
0.0089	62.27	19.95	42.32	39.41	0.052	2.1	8.36
0.0089	62.27	19.95	42.32	39.41	0.105	1.76	7.14
0.0089	62.27	19.95	42.32	39.41	0.183	1.72	6.03
0.0089	62.27	19.95	42.32	42.44	0.052	2.1	9.196
0.0089	62.27	19.95	42.32	42.44	0.183	1.72	6.56
0.0089	62.27	19.95	42.32	45.47	0.052	2.1	10.032
0.0089	62.27	19.95	42.32	45.47	0.101	1.76	8.698
0.0089	62.27	19.95	42.32	45.47	0.115	1.74	8.1
0.0089	62.27	19.95	42.32	45.47	0.184	1.72	7.08
0.0089	62.27	19.95	42.32	45.47	0.233	1.7	6.5
0.2663	104.02	35.47	68.55	39.41	0.052	2.1	8.36
0.2663	104.02	35.47	68.55	39.41	0.101	1.76	7.14
0.3915	70.814	24.864	45.95	42.44	0.103	1.76	7.924
0.3915	70.814	24.864	45.95	42.44	0.183	1.72	6.56
0.3915	70.814	24.864	45.95	45.47	0.183	1.72	7.08
0.108	78.08	18.09	59.99	39.41	0.052	2.1	8.36
0.108	78.08	18.09	59.99	39.41	0.183	1.72	6.03

0.108	78.08	18.09	59.99	42.44	0.183	1.72	6.56
0.108	78.08	18.09	59.99	42.44	0.210	1.7	6.06
0.108	78.08	18.09	59.99	45.47	0.105	1.76	8.698
0.108	78.08	18.09	59.99	45.47	0.183	1.72	7.08
0.108	78.08	18.09	59.99	45.47	0.256	1.68	7.01
0.218	83.55	22.08	61.47	39.41	0.052	2.1	8.36
0.218	83.55	22.08	61.47	42.44	0.052	2.1	9.196
0.218	83.55	22.08	61.47	42.44	0.105	1.76	7.924
0.218	83.55	22.08	61.47	42.44	0.120	1.75	6.924
0.218	83.55	22.08	61.47	45.47	0.052	2.1	10.032
0.218	83.55	22.08	61.47	45.47	0.105	1.76	8.698
0.218	83.55	22.08	61.47	45.47	0.128	1.75	7.28
0.406	78.66	18.94	59.72	42.44	0.105	1.76	7.924
0.406	78.66	18.94	59.72	45.47	0.052	2.1	10.032
0.549	91.49	32.82	58.67	39.41	0.052	2.1	8.36
0.549	91.49	32.82	58.67	39.41	0.105	1.76	7.14
0.549	91.49	32.82	58.67	42.44	0.052	2.1	9.196
0.549	91.49	32.82	58.67	42.44	0.105	1.76	7.924
0.549	91.49	32.82	58.67	45.47	0.052	2.1	10.032
0.549	91.49	32.82	58.67	45.47	0.105	1.76	8.698
0.549	91.49	32.82	58.67	45.47	0.183	1.72	7.08

865